A Marked Point Process Model Incorporating Active Contours Boundary Energy

Camilo Aguilar, Mary Comer
Purdue University, West Lafayette, IN, USA

Abstract

In this paper we incorporate an active contours energy into the Marked Point Process (MPP) framework. The addition of this energy allows the MPP model to detect objects with irregular shapes. This energy accounts for the elasticity and curvature properties of the detected objects. We employ the balloon method to prevent the contour from stagnating at local minima. We use calculus of variations to evolve each individual contour and we use stochastic multiple birth and death dynamics to optimize the MPP energy function. We demonstrate that our method successfully models components with irregular shape in material images, but the model can be extended to other applications.

Introduction

The Marked Point Process Framework(MPP) has became a powerful tool in image analysis. It exploits the geometric properties of certain systems to model a scene as a configuration of objects. This method has been implemented in both material and biological images. For example, Craciun et al. proposed an efficient ellipse model to detect and track images of biological cells in [1]. Similarly, Gadgil et al. used the disk model to detect nuclei in [2]. Zhao et al. proposed a unified ellipse MPP model together with a Markov Randon Field framework to analyze NiCrAl particles in [3]. All of these methods successfully characterized images comprised of repeated patterns. However, some systems require analysis of more complex shapes without a pre-defined geometry. For example, Figure 1 shows two images of a fiber reinforced polymer. This system is composed of glass fibers, polymer matrix, and voids. Li et al. proposed in [4] a Multimark MPP with segments and ellipses that models fibers successfully. However, voids represent a more challenging task due to two reasons: they often have an irregular geometry and they do not have a constant pixel intensity. These factors can cause problems in segmentation algorithms that rely on pixel intensities such as watershed or MRF based segmentations, as shown in Figure 2(a).

On the other hand, contour-based detection methods have shown promising results for detecting individual voids. Figure 2(b) denotes the resulting contour from applying the balloon model proposed by Cohen in [5] on a single void. Kulikova et al in [6] successfully incorporated the active contours framework into an MPP configuration to model objects with irregular shapes. This method evolved contours based on contour smoothness, image edges and precomputed background and foreground intensities. However that approach would not yield satisfactory results on images such as Figure 2(b) due to the similar intensities between the object foreground and background.

Our method aims to extend the work presented in [6] by incorporating a different optimization technique. We also use differ-
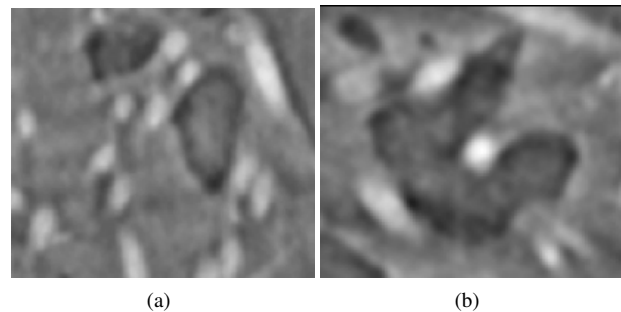

Figure 1. *Example of irregularly-shaped objects: Fiber reinforced composite polymer. Fibers(white), Voids(dark), Matrix(gray). Courtesy of The Advanced Computational Materials and Experimental Evaluation Lab, Purdue University.*
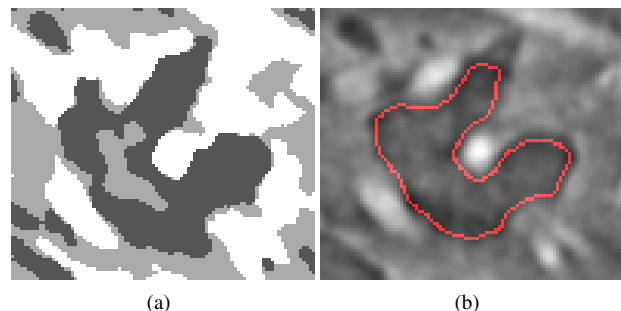

Figure 2. *Example different detection/segmentation algorithms. (a) The EMMPM with 3 classes: Fibers(white), Voids(dark), Matrix(gray). (b) Active Contours used to detect voids*

ent forces such as the balloon force proposed by [5], and a pre-segmentation energy. These changes allow the MPP-Active Contours Framework to detect a larger range of objects while modeling the object structural characteristics.

Contour Energy

We model an individual object as a closed contour denoted by $C(t) = (x(t), y(t))$, $t \in [0, 2\pi]$. This contour is defined on the image domain and is deformed according to the energy functional $E(C(t))$ given by:

$$E(C(t)) = \int_0^{2\pi} \frac{1}{2} (\alpha ||C'(t)||^2 + \beta ||C''(t)||) + E_{ext}(C(t)) \, dt \quad (1)$$

In this equation, $C'(t)$ and $C''(t)$ denote the first and second derivative of the contour with respect to parameter t. These terms model the object elasticity and curvature respectively and they

are regulated by the positive parameters α and β. During all the methods described in the paper, we set the parameters $\alpha, \beta \in [0, 1]$.

External Energy

The external energy defines the fitting of the snake with the image and it is defined by:

$$E_{ext}(C(t)) = E_{Edge}(C(t)) + E_{dark}(C(t)) \qquad (2)$$

The first term attracts the contour towards image edges and it is given by $E_{Edge} = -||\nabla(g_\sigma * I(x(t), y(t)))||^2$, where g_σ is a Gaussian smoothing filter with parameter σ and ∇ is the gradient operator. The second term is a pre-segmentation energy and it is defined as : $E_{dark} = I_k(x(t), y(t))$, where I_k is zero everywhere except at the output for a pre-segmentation algorithm. For example, in Figure 2(a),the class of interest is the void region, therefore we chose class $k = 1$, the one with lowest pixel intensity values. We used the EM/MPM segmentation proposed in [7] as a pre-segmentation algorithm.

Finally, We used the method proposed in [5] to ensure the contour will evolve even when it is not subject to an external force. This force contributes to the characterization of irregular objects that do not have a constant internal pixel intensity. The balloon force is given by: $F_{balloon} = \kappa \hat{n}(t)$, where κ is a positive constant and $\hat{n}(t)$ represents the normal vector to the contour.

Boundary Energy Optimization

We employed calculus of variations to find a force-balanced equation. The solution to this method is expressed as the Euler-Lagrange equations given by: $\alpha C''(t) - \beta C''(t) - \nabla E_{ext} = 0$. The numerical approximation for this equation is discussed in [8] and its solution is given by:

$$C^k(t) = (A + \gamma I)^{-1}(\gamma C^{k-1}(t) - \nabla E_{ext}(C^{k-1}(t)) \qquad (3)$$

Where $C^k(t)$ denotes the contour at iteration k, γ represents the step size or viscosity parameter , Matrix A denotes a pentadiagonal matrix containing the discrete approximations of the first and second derivative coefficients, and ∇E_{ext} denotes the gradient of the external energy.

Note that the external force includes the balloon force to inflate the contour together with three positive constants $\kappa_1, \kappa_2, \kappa_3$ to weight the effect of each individual force: $\nabla E_{Ext} = \kappa_1 \hat{n} - \kappa_2 \nabla E_{edge} - \kappa_3 \nabla E_{dark}$. In our experiments, we used $\kappa_1 = 0.5$, $\kappa_2 = 1$ and $\kappa_3 = 0.1$, and [5] recommended to choose each κ within the same order of magnitude.

A Marked Point Process with Active Boundary Energy
Marked Point Process Framework

A Marked Point Process $\mathbf{W}$ defined on $K \times M$ models the observed scene Y as a finite unordered set of random objects. The positions of these objects are defined on the compact space $K = [0, X_{min}] \times [0, Y_{max}] \subset R^2$ and their geometry and dimensions are determined by the mark space M. For example, the mark space for the disk model is defined as: $M = [r_{min}, r_{max}]$, where r describes the disk's radius. A single object is denoted $\omega_i = (k_i, m_i)$, where $k_i \in K$ and $m_i \in M$. We say a realization of the MPP $\mathbf{W}$ is defined by $\mathbf{w} = \{\omega_1, \omega_2, ..., \omega_n\} \in \Omega_w$ where $\mathbf{w}$ denotes the configuration of n random objects, ω_i is a single object, and Ω_w

denotes the space of all possible realizations of $\mathbf{W}$. The point process can be modeled by a conditional Gibbs density function given by

$$p(\mathbf{w}|y) = \frac{1}{Z} \exp\{-U(\mathbf{w}|y)\} \qquad (4)$$

where the observed image y describes a realization of Y, $U(\mathbf{w}|y)$ describes the energy function and $Z = \int_{\mathbf{W} \in \Omega_w} p(\mathbf{w}|y)d\mathbf{w}$ is the normalizing constant.

Irregular Shape Marked Point Process

The addition of active contours boundary would require a high dimensional mark space to represent irregular geometries. However, Kulikova presented in [6] an alternative space to represent these configurations based on the disk MPP model and the contour energy functional $E(C(t))$. We let an initial disk ω_i with radius r_i belong to space $\mathbf{W} = K \times M$. We can parametrize a disk ω_i as a contour $\omega_i(t)$ living in a space W_o and define a contour energy functional $E(\omega_i(t))$. We can minimize this functional using the method described in section to evolve $\omega_i(t)$ into $\tilde{\omega}_i(t) \in W_o$, with $\tilde{~} : W_o \mapsto W_o$ denoting the energy minimization(and following the notation of [6]). Therefore, the new single object space is defined as $W_o = \tilde{W}$. This space describes the contour initialized by ω_i adapted to the image by a local minimum of $E(\omega(t))$.

We followed [6] to create the extension from a single object to multiple objects, given by the symmetrical set:

$$\Omega_{W_o} = \bigcup_{n=0}^{\infty} [W_o^n / S_n], \qquad (5)$$

where S_n is a symmetry group of n elements on the components of the product. The energy of this MPP model is described as:

$$U(\mathbf{w}|y) = \sum_{\omega_i \in \mathbf{w}} U_d(\omega_i|y) + \sum_{\omega_i, \omega_j \in \mathbf{w}} U(\omega_i, \omega_j) \qquad (6)$$

Where U_d denotes the data energy and U_p denotes the prior energy.

Data Energy

The data energy describes how well current configuration $\mathbf{w}$ fits with the current image and it is the sum of all the individual data energies for each object ω_i. The data energy for a single object is given by:

$$U_d(\omega_i|y) = E(\tilde{\omega}_i(t)) \qquad (7)$$

Prior Energy

This energy $U_p(\mathbf{w})$ accounts for prior knowledge about the system. Numerous MPP models use an overlapping penalizer which discourages spatial overlap between detected objects in $\mathbf{w}$. Hence, our prior energy depends only on the interaction between objects:

$$U_p(\omega_i, \omega_j) = \left\{ \begin{array}{ll} A(\tilde{\omega}_i, \tilde{\omega}_j) & if \quad A(\tilde{\omega}_i, \tilde{\omega}_j) \leq T_{overlap} \\ \infty & otherwise \end{array} \right\} (8)$$

Where $A(\tilde{\omega}_i, \tilde{\omega}_j)$ denotes the overlapping ratio between $\tilde{\omega}_i$ and $\tilde{\omega}_j$. For this section, we chose $T_{overlap} = 5\%$ experimentally in order to prevent from multiple contours converging to the same local minimum.

Optimization

Our objective is to obtain the MAP estimate of equation (4) by minimizing the energy function given in equation (6). This energy function is not convex and also it is numerically infeasible to calculate the normalizing constant $Z = \int_{\mathbf{W} \in \Omega_w} p(\mathbf{w}|y) \, d\mathbf{w}$. Hence we resort to stochastic optimization embedded in a simulated annealing scheme. We simulate a Markov Chain from Ω_W and use the multiple birth and death dynamics presented by [9] . This algorithm uses a pre-computed birthmap to favor certain regions during the birthphase and gives birth to multiple objects in each iteration. Then it sorts the detected objects by decreasing energy to "kill" the less likely objects first. Finally it decreases the temperature T and the process intensity σ to ensure convergence to a strong local minimum. This optimization method is summarized in Algorithm 1.

Algorithm 1 Multiple Birth and Death Algorithm

1: **procedure** MPP ENERGY MINIMIZATION
2:     *Initialization*:
3:     Create birthmap b_o
4:     Initialize $b_{rate} = b_o$, $T = T_o$, $\sigma = \sigma_o$.
5:     *Birth Step*:
6:     Visit pixels in raster order
7:     $\omega' \leftarrow$ draw a sample from space W
8:     Add ω' to configuration $\mathbf{w}$ with probability σb_{rate}
9:     Evolve ω' using the method described in section to $\tilde{\omega}'$
10:     *Death Step*:
11:     Sort all elements of $\mathbf{w}$ by decreasing energy.
12:     For every object ω_i in $\mathbf{w}$ calculate:
13:     $d_{rate}(w_i) = \dfrac{\sigma^{(k)} exp \frac{U(\mathbf{W}|Y) - U(\mathbf{W} - \omega_i|Y)}{T^k}}{1 + \sigma^{(k)} exp \frac{U(\mathbf{W}|Y) - U(\mathbf{W} - \omega_i|Y)}{T^k}}$;
14:     Delete ω_i with probability $d_{rate}(\omega_i)$
15:     *Convergence Test*:
16:     **if** all the elements born during the birth step are killed during the death step **then**
17:         terminate process
18:     **else**
19:         Update parameters: $T^{k+1} \leftarrow T^k \times \alpha$, $\sigma^{k+1} \leftarrow \sigma^k \times \alpha$ $\alpha \in (0,1)$
20:         **goto** *Birth Step*
21:     **end if**
22: **end procedure**

Results and Experiments

We tested our model on two different datasets: a fiber reinforced polymer and a Pb-Sn alloy, and we compared it with the software provided by [10].

Void Detection in Fiber Reinforced Polymer

Figure 3 represents a fiber reinforced polymer described in [11]. It belongs to a 4D (volume and time) dataset and is composed of three classes: matrix(gray), fibers(white) and voids(dark/gray). Figure 3(c) shows that our algorithm can effectively characterize the largest voids despite their irregular internal pixel intensity. The birthmap used for this data was a dilated image of the 10% of darkest pixels. We exploited E_{dark} to ensure that contours with dark edges have low energy. Figure 3(b) shows
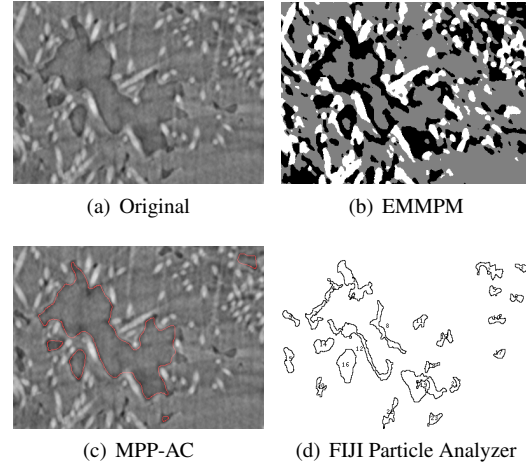

(a) Original   (b) EMMPM

(c) MPP-AC   (d) FIJI Particle Analyzer

Figure 3. *Void Detection on Fiber Reinforced Polymer, courtesy of Dr. Michael Sangid, Purdue University*

the EM/MPM results using 3 classes. This algorithm can detect the contour of the void but the interior region is labeled as background. Figure 3(d) shows the results of using FIJI's[10] particle analyzer tool.

Pb-Sn Dendrite Alloy:

(a) Original   (b) EMMPM

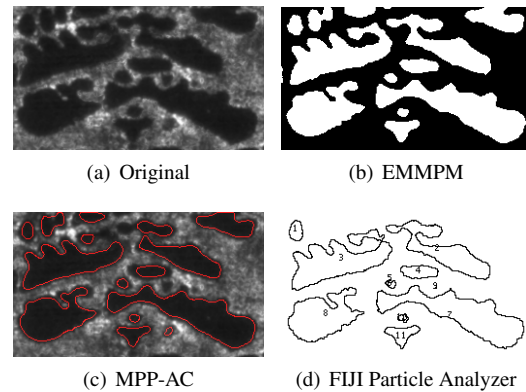(c) MPP-AC   (d) FIJI Particle Analyzer

Figure 4. *Dendrite Detection on Pb-Sn Alloy. Courtesy of Dr. Peter Voorhees, Northwestern University*

Figure 4 shows Pb-Sn dendrites described in [12].This study focused on characterizing dendritic morphology. Figure 4(c) shows that our model fits the majority of objects. However, the balloon method has drawbacks in objects close to each other, such as those shown in the upper left part of the image where the contour merged two nearby objects together. This issue can be addressed by improving the contour energy model and be explored in future research. Figures 4(b) and 4(d) show the results of EM/MPM and FIJI particle analyzer.

Conclusion and Discussion

In this paper we explored a method to incorporate the boundary energy to the Marked Point Process. Our model combines the balloon model active contours with the MPP framework. This combinations allows the MPP to model material im-

age properties while detecting objects with irregular shapes or non-homogeneous intensities. Although we focused on detecting voids dataset in Figure 3, we demonstrated that our method can be applied to a different dataset. This model can be extended to 3D datasets.

Acknowledgment

References

[1] P. Craciun, "Stochastic Geometry for Automatic Multiple Object Detection and Tracking in Remotely Sensed High Resolution Image Sequences," Ph.D. dissertation, Universit Nice Sophia Antipolis, 2016.

[2] N. J. Gadgil, W. Lafayette, P. Salama, K. W. Dunn, and E. J. Delp, "Nuclei Segmentation of Fluorescence Microscopy Images Based on Midpoint Analysis and Marked Point Process," pp. 37–40, 2016.

[3] H. Zhao, "Combining Markov Random field and Marked Point Process for Microscopy Image Modeling," Ph.D. dissertation, Purdue University, 2016.

[4] T. Li, M. Comer, and J. Zerubia, "A connected tube model for marked point process," 2018, manuscript submitted for publication: IEEE International Conference on Image Processing (ICIP).

[5] L. D. Cohen and I. Cohen, "Finite Element Methods for Active Contour Models and Balloons for 2D and 3D Images," *Pattern Analysis and Machine Intelligence, IEEE Transactions on*, no. November, pp. 1131–1147, 1993.

[6] M. Kulikova, I. Jermyn, X. Descombes, J. Zerubia, and E. Zhizhina, "A marked point process model with strong prior shape information for the extraction of multiple, arbitrarily-shaped objects," *Proceedings - 5th International Conference on Signal Image Technology and Internet Based Systems, SITIS 2009*, pp. 180–186, 2009.

[7] M. L. Comer and E. J. Delp, "The EM/MPM algorithm for segmentation of textured images: Analysis and further experimental results," *IEEE Transactions on Image Processing*, vol. 9, no. 10, pp. 1731–1744, 2000.

[8] M. Kass, A. Witkin, and D. Terzopoulos, "Snakes: Active contour models," *International Journal of Computer Vision*, vol. 1, no. 4, pp. 321–331, 1988.

[9] X. Descombes, R. Minlos, and E. Zhizhina, "Object extraction using a stochastic birth-and-death dynamics in continuum To cite this version : Object extraction using a stochastic birth-and-death dynamics in continuum," 2009.

[10] J. Schindelin, I. Arganda-Carreras, E. Frise, V. Kaynig, M. Longair, T. Pietzsch, S. Preibisch, C. Rueden, S. Saalfeld, B. Schmid, J.-Y. Tinevez, D. J. White, V. Hartenstein, K. Eliceiri, P. Tomancak, and A. Cardona, *Fiji: an open-source platform for biological-image analysis*, 06 2012. [Online]. Available: http://dx.doi.org/10.1038/nmeth.2019

[11] R. F. Agyei, B. Sharma, and M. Sangid, "Investigating Sub-surface Microstructure in Fiber Reinforced Polymer Composites via X-Ray Tomography Characterization," *57th AIAA/ASCE/AHS/ASC Structures, Structural Dynamics, and Materials Conference*, no. January, pp. 1–6, 2016. [Online]. Available: http://arc.aiaa.org/doi/10.2514/6.2016-0409

[12] T. Cool and P. W. Voorhees, "The evolution of dendrites during coarsening: Fragmentation and morphology," *Acta Materialia*, vol. 127, pp. 359–367, 2017. [Online]. Available: http://dx.doi.org/10.1016/j.actamat.2017.01.029

Author Biography

Camilo Aguilar received his BS in Electrical Engineering at the University of California Irvine in 2015. He is currently working on his PhD at Purdue University, West Lafayette, in the field of Image Processing.

Mary L. Comer (S'91M'92SM'96) received the B.S., M.S., and Ph.D. degrees from Purdue University, West Lafayette, IN, in 1990, 1993, and 1995, respectively, all in electrical engineering.

From 1992 until 1995, she held a National Science Foundation Graduate Fellowship. From 1995 until 2005, she was with Thomson, Indianapolis, IN, where she was a Senior Member of the Technical Staff in the Corporate Research Division. While at Thomson, she was involved with video coding, multiresolution video, and video postprocessing for applications including high-definition DVD, Internet video, satellite television, and security and surveillance. Dr. Comer was a participant and contributor to the HD-DVD Forum committee tasked with recommending a video coding standard for high-definition video on red laser DVD discs. She served as Demo Co-Chair for the 2007 IEEE International Symposium on Multimedia (ISM). She currently serves as an Associate Editor for the IEEE Transactions on Circuits and Systems for Video Technology.

Currently, she is an Associate Professor at the School of Electrical and Computer Engineering, Purdue University. Her research interests include statistical image modeling, texture-based segmentation of images, medical imaging, analysis of microstructural images and multi-resolution/scalable video coding.